A Real-Time Optimization with Warm-Start of Multiperiod AC Optimal Power Flows

Youngdae Kim and Mihai Anitescu
Mathematics and Computer Science Division
Argonne National Laboratory
Lemont, IL, USA
{youngdae,anitescu}@mcs.anl.gov

***Abstract*—We present a real-time optimization strategy based on warm-start for solving a moving horizon of multiperiod AC optimal power flow (ACOPF) problems. In each horizon, ACOPFs are temporally interlinked via generator ramp constraints, and we assume that each horizon needs to be solved every few seconds or minutes. We introduce two approximate tracking schemes that closely follow a solution path consisting of strongly regular points. We present theoretical results bounding the tracking error by the square of the parameter changes between time periods. Experimental results for networks of sizes up to 9K buses show a fast computation time while maintaining a good solution quality, thus making our approach well suited for real-time circumstances.**

***Index Terms*—multiperiod AC OPFs, real-time optimization, moving horizon, parametric optimization**

I. Introduction

In a multiperiod AC optimal power flow (ACOPF) model [1], [2], [3], [4], [5], we optimize inter-temporally coupled ACOPF problems over a time horizon consisting of multiple time periods: an ACOPF containing network AC power balance and flow limit constraints is defined at each time period, and ACOPFs in different time periods are coupled through time-coupling constraints specifying physical requirement over time, such as generator ramp rate and energy storage state. These temporal constraints enable us to model the effect of the current decision on future system state and decisions. Under these domain and temporal constraints, the model seeks an optimal generation dispatch for the current time period that is optimized over a time horizon.

The control feature of the multiperiod model – taking into account the impact of the current decision on future decisions – plays an important role in scheduling a reliable and economical generator operation over a time horizon [2], [4]. This feature is especially critical in emergency situations, such as a loss of a large generator, where we should provide a reliable generator operation satisfying load until the system recovers to its normal state. For example, in emergency, a spinning reserve starts to be used to make up for insufficient generation, which leaves less headroom for generator capacity. In this case, considering just a single time period may result in some generators being close to their capacity. Subsequently, at the next time period other generators may be required to generate more than their ramp rate, which leads to an infeasible generator operation. The multiperiod model that takes into account generator ramp rate can avoid this situation and provide a reliable generation dispatch.

Mathematically, the multiperiod problem considered in this paper is defined as follows:

$$
\begin{aligned}
\underset{v_{t,i},\theta_{t,i},p_{t,g},q_{t,g}}{\text{minimize}} \quad & \sum_{t\in\mathcal{T}}\sum_{g\in\mathcal{G}} f_g(p_{t,g}),\\
\text{subject to}\quad & \sum_{g\in\mathcal{G}_i} p_{t,g} - d^p_{t,i} = \sum_{(i,k)\in\mathcal{L}} p_{t,ik} + \sum_{(k,i)\in\mathcal{L}} p_{t,ki} + g^s_i v^2_{t,i},\\
& \sum_{g\in\mathcal{G}_i} q_{t,g} - d^q_{t,i} = \sum_{(i,k)\in\mathcal{L}} q_{t,ik} + \sum_{(k,i)\in\mathcal{L}} q_{t,ki} - b^s_i v^2_{t,i},\\
& \qquad\qquad \forall t\in\mathcal{T}, \forall i\in\mathcal{B},\\
& p_{t,ik} = g^c_{ik} v^2_{t,i} + v_{t,i}v_{t,k}(g_{ik}\cos(\theta_{t,ik}) + b_{ik}\sin(\theta_{t,ik})),\\
& q_{t,ik} = -b^c_{ik} v^2_{t,i} + v_{t,i}v_{t,k}(g_{ik}\sin(\theta_{t,ik}) - b_{ik}\cos(\theta_{t,ik})),\\
& p_{t,ki} = g^c_{ki} v^2_{t,k} + v_{t,i}v_{t,k}(g_{ki}\cos(\theta_{t,ki}) + b_{ki}\sin(\theta_{t,ki})),\\
& q_{t,ki} = -b^c_{ki} v^2_{t,k} + v_{t,i}v_{t,k}(g_{ki}\sin(\theta_{t,ki}) - b_{ki}\cos(\theta_{t,ki})),\\
& \theta_{t,ik} := \theta_{t,i} - \theta_{t,k}, \theta_{t,ki} := \theta_{t,k} - \theta_{t,i}, \forall t\in\mathcal{T}, \forall (i,k)\in\mathcal{L},\\
& \sqrt{p^2_{t,ik} + q^2_{t,ik}} \le s_{ik}, \qquad \forall t\in\mathcal{T}, \forall (i,k)\in\mathcal{L},\\
& \sqrt{p^2_{t,ki} + q^2_{t,ki}} \le s_{ki}, \qquad \forall t\in\mathcal{T}, \forall (i,k)\in\mathcal{L},\\
& |p_{t+1,g} - p_{t,g}| \le r_g, \qquad \forall t\in\mathcal{T}\backslash\{T\}, \forall g\in\mathcal{G},\\
& \underline{v}_i \le v_{t,i} \le \overline{v}_i, \qquad \forall t\in\mathcal{T}, \forall i\in\mathcal{B},\\
& \underline{\theta}_i \le \theta_{t,i} \le \overline{\theta}_i, \qquad \forall t\in\mathcal{T}, \forall i\in\mathcal{B},\\
& \underline{p}_g \le p_{t,g} \le \overline{p}_g, \qquad \forall t\in\mathcal{T}, \forall g\in\mathcal{G},\\
& \underline{q}_g \le q_{t,g} \le \overline{q}_g, \qquad \forall t\in\mathcal{T}, \forall g\in\mathcal{G}.
\end{aligned}
\tag{1}
$$

In (1), $\mathcal{T}, \mathcal{B}, \mathcal{G}$, and $\mathcal{L}$ denote the sets of time periods, buses, generators, and branches, respectively. The set $\mathcal{T}$ is assumed to be $\{1,\dots,T\}$ representing a sequential order of time periods. $\mathcal{G}_i$ denotes a set of generators connected to bus i. For each $(i,k) \in \mathcal{L}$, i is a from-bus, and k is a

This material is based upon work supported by the U.S. Department of Energy, Office of Science, under contract DE-AC02-06CH11357. MA acknowledges partial NSF funding through awards FP061151-01-PR and CNS-1545046.

to-bus. Parameters $g^c_{ik}, g_{ik}, g^c_{ki}, g_{ki}, b^c_{ik}, b_{ik}, b^c_{ki}$, and b_{ki} are from complex admittance matrix containing the complex series admittance and branch shunt, g^s_i and b^s_i are from bus shunt, s_{ik} and s_{ki} are apparent power limits, and $d^p_{t,i}$ and $d^q_{t,i}$ represent the loads for real and reactive power at bus i at time period t, respectively. Variables, $v_{t,i}, \theta_{t,i}, p_{t,g}$, and $q_{t,g}$, contain voltage magnitude, voltage angle, real power, and reactive power values at each bus or generator at time period t, respectively.

In this paper, we consider a real-time optimization strategy for solving a moving horizon problem of multiperiod AC optimal power flows (MPACOPFs). Specifically, we solve a single time horizon consisting of an MPACOPF with a fixed length of time periods, $|\mathcal{T}| = T$. The horizon then moves forward one time period with a new load corresponding to the incoming time period, and we repeat the procedure. We aim for a fast approximate computation strategy that exhibits a good solution quality so that it can provide an accurate solution feedback for each horizon in real time, defined here to be less than a second for smaller networks of sizes up to 300-bus or less than two minutes for larger ones of sizes up to 9K-bus when $T = 10$. As we describe in Section IV, our computation time is comparable to the one for real-time optimization of a single period OPF [6]. This fast computation time is critical in an emergency where the restoration phase should establish a reliable and economic generator operation quickly within a specific time limit. Our real-time strategy will enable fast deployment of the model and to reflect the most recent information about load as time goes.

To achieve real-time performance, we introduce a tracking scheme combined with warm-start. Our scheme exploits (i) the solution overlap of two consecutive horizons by warm-start and (ii) the real-time requirement where parameter changes, such as load changes, are expected to be small between adjacent horizons.

Specifically, we present two warm-start methods exploiting the solution at the previous time horizon to generate a good initial point for the current time horizon. An error analysis based on the Karush-Kuhn-Tucker (KKT) conditions provides insights into factors dominating quality control and criteria for selecting the warm-start method.

Moreover, we accelerate computation further by approximately following a solution manifold consisting of strongly regular points [7]. Based on our previous work [8], we present theoretical results showing that a quadratic programming (QP) solve (sometimes, only one Newton iteration of perturbed KKTs) may be enough to have an approximate solution whose error is bounded by the square of the parameter changes at the last time period. Experimental results are given for networks of sizes up to a 9K bus system demonstrate the real-time performance of our approximate tracking scheme.

The rest of the paper is organized as follows. Section II introduces two different warm-start methods with their KKT error analysis. Section III presents our approximate tracking scheme and shows that its errors are bounded to the square of parameter changes between time periods. Computational results are described in Section IV, and Section V concludes the paper. We note that due to space limitation we omit all our proofs. Interested readers are referred to [9] for the proofs.

II. Warm-start

In this section, we introduce our two warm-start methods for real-time computation of MPACOPFs along with their error analysis. We start with our abstraction of the AC polar formulation (1) for analysis purposes.

$$\begin{aligned} \underset{x,s}{\text{minimize}} \quad & \sum_{t\in\mathcal{T}} f(x_t), \\ \text{subject to} \quad & h(x_t) = d_t,\ \forall t \in \mathcal{T}, \\ & c(x_t) \le 0,\ \forall t \in \mathcal{T}, \\ & x_{t+1,g} - x_{t,g} = s_{t,g},\ \forall t \in \mathcal{T}\backslash\{T\}, \forall g \in \mathcal{G}, \\ & l^x \le x_t \le u^x,\ \forall t \in \mathcal{T}, \\ & l^s \le s_t \le u^s,\ \forall t \in \mathcal{T}\backslash\{T\}, \end{aligned} \tag{2}$$

where variables at time period t are encapsulated in x_t. We assume that the first $|\mathcal{G}|$ elements of x_t correspond to the real power generator variable $p_{t,g}$, i.e., $x_{t,g} := p_{t,g}, \forall g \in \mathcal{G}$. The objective function $f(x_t)$ represents the aggregated generators' cost at time period t. The constraint $h(\cdot)$ corresponds to the power balance equations satisfying the given load denoted by d_t, and $c(\cdot)$ encapsulates the line flow limits. The ramping values are identified with variable s_t, denoting a vector of variables $s_{t,g}$'s, and the ramp limit is represented by its lower and upper bounds. We note that the objective function and constraints are time invariant. This feature will be exploited in our warm-start.

Since the problem (2) is nonconvex (mainly because of the nonlinearity of the power balance equations), we find its solution by computing a stationary point, where there are no feasible descent directions for the gradient of the objective function. Under suitable constraint qualifications, such as the linear independence constraint qualification (LICQ) or Mangasarian-Fromovitz constraint qualification (MFCQ) [10], this is equivalent to finding a point satisfying the KKT conditions as described in (3) below. We call such a primal/dual pair a KKT point. We sometimes omit the dual part when we specify a KKT point. Throughout this paper, a solution is assumed to be optimal if it is a KKT point.

$$\begin{aligned} &\nabla f(x_t) + \nabla h(x_t)\lambda_t + \nabla c(x_t)\mu_t \\ &\quad +W_t(\omega) - z^{x,l}_t + z^{x,u}_t = 0, \quad \forall t \in \mathcal{T}, && \text{(3a)} \\ &\quad -\omega_t - z^{s,l}_t + z^{s,u}_t = 0, \quad \forall t \in \mathcal{T}\backslash\{T\}, && \text{(3b)} \\ &\quad h(x_t) - d_t = 0, \quad \forall t \in \mathcal{T}, && \text{(3c)} \\ &\quad x_{t+1,g} - x_{t,g} - s_{t,g} = 0, \quad \forall t \in \mathcal{T}\backslash\{T\}, \forall g \in \mathcal{G}, && \text{(3d)} \\ &\quad 0 \le -c(x_t) \perp \mu_t \ge 0, \quad \forall t \in \mathcal{T}, && \text{(3e)} \\ &\quad 0 \le (x_t - l^x) \perp z^{x,l}_t \ge 0, \quad \forall t \in \mathcal{T}, && \text{(3f)} \\ &\quad 0 \le (u^x - x_t) \perp z^{x,u}_t \ge 0, \quad \forall t \in \mathcal{T}, && \text{(3g)} \\ &\quad 0 \le (s_t - l^s) \perp z^{s,l}_t \ge 0, \quad \forall t \in \mathcal{T}\backslash\{T\}, && \text{(3h)} \\ &\quad 0 \le (u^s - s_t) \perp z^{s,u}_t \ge 0, \quad \forall t \in \mathcal{T}\backslash\{T\}, && \text{(3i)} \end{aligned}$$

where

$$W_t(\omega) = \begin{cases} E(-\omega_1) & \text{if } t = 1, \\ E(\omega_{t-1} - \omega_t) & \text{if } t \in \mathcal{T}\backslash\{1, T\}, \\ E(\omega_{T-1}) & \text{if } t = T, \end{cases} \quad E = \begin{bmatrix} I \\ 0 \end{bmatrix}, \quad I : \text{a } |\mathcal{G}|\text{-by-}|\mathcal{G}| \text{ identity matrix} \tag{4}$$

Note that the complementarity notation $0 \le a \perp b \ge 0$ implies that $a, b \ge 0$ and $\sum_i a_i b_i = 0$. $\omega_{t,g}$ is a multiplier for the ramp constraint of generator g between time periods t and $t+1$. If the ramping is not binding, that is, $l^s_{t,g} < s_{t,g} < u^s_{t,g}$, then $z^{s,l}_{t,g} = z^{s,u}_{t,g} = 0$ from (3h) and (3i). Thus $\omega_{t,g} = 0$ from (3b) in this case. Otherwise, $\omega_{t,g}$ takes either a nonpositive or a nonnegative value depending on the ramp constraints being bound at its lower or upper limit, respectively.

A. Construction of a warm-start point

We consider an initial point computation for the second time horizon problem. For future time horizons with a starting time period $t \ge 3$, we recursively apply our method based on the solution of the previous time horizon problem.

For the second time horizon problem, we need to modify its problem structure to incorporate the ramping decisions made in the first time horizon. Assume that $(\tilde{x}, \tilde{s}, \tilde{\lambda}, \tilde{\mu}, \tilde{\omega}, \tilde{z}^x, \tilde{z}^s)$ is a solution to (3) for the first time horizon. The second time horizon problem is constructed by shifting and moving forward in time (thus the first time period goes away) and introducing a new time period $(T+1)$ at the end with its load d_{T+1}. Although there is no time period 1, its ramp constraints should be satisfied since the generators are assumed to have operated with the value of $\tilde{x}_{1,g}$. Note that for a fixed value of $\tilde{x}_{1,g}$ the ramp constraint is nothing but a bound constraint on $x_{2,g}$. Therefore, we update the lower and upper bounds of $x_{2,g}$ to incorporate the ramping decisions:

$$\begin{aligned} l^x_{2,g} &= \max(l^x_{2,g}, \tilde{x}_{1,g} + l^s_g), \\ u^x_{2,g} &= \min(u^x_{2,g}, \tilde{x}_{1,g} + u^s_g). \end{aligned} \tag{5}$$

Based on the modifications, we construct our warm-start point by first forming a KKT point for the smaller horizon $\{2, \ldots, T\}$ problem and then choosing appropriate values for the new variables for time period $(T+1)$.

With the updated bounds on x_2 and by the Bellman's principle of optimality, one can easily verify that $(\tilde{x}_{2:T}, \tilde{s}_{2:(T-1)})$ is an optimal solution to the smaller horizon $\{2, \ldots, T\}$ problem. However, the existing multipliers $(\tilde{\lambda}, \tilde{\mu}, \tilde{\omega}, \tilde{z}^x, \tilde{z}^s)$ may not satisfy the KKT conditions since ω_1 is no longer available. Specifically, $W_2(\omega) = E(\omega_1 - \omega_2)$ is now changed to $E(-\omega_2)$. If $\tilde{\omega}_1 \ne 0$, then (3a) is not satisfied for $t = 2$. Since ω works as if it is a multiplier on a bound constraint for a fixed real power generation, we can easily fix this by absorbing the value of $\tilde{\omega}_1$ in the dual variable z^x_2 using the following update rule:

$$\begin{aligned} \tilde{z}^{x,l}_{2,g} &= \begin{cases} \tilde{z}^{x,l}_{2,g} - \tilde{\omega}_{1,g} & \text{if } \tilde{x}_{2,g} = \tilde{x}_{1,g} + l^s_g, \\ \tilde{z}^{x,l}_{2,g} & \text{otherwise,} \end{cases} \\ \tilde{z}^{x,u}_{2,g} &= \begin{cases} \tilde{z}^{x,u}_{2,g} + \tilde{\omega}_{1,g} & \text{if } \tilde{x}_{2,g} = \tilde{x}_{1,g} + u^s_g, \\ \tilde{z}^{x,u}_{2,g} & \text{otherwise.} \end{cases} \end{aligned} \tag{6}$$

Note that the changes made in (6) do not affect other KKT conditions except for (3a), (3f), and (3g) since $\tilde{z}^x$ is not an intertemporal variable. Also, the newly updated values are nonnegative. For example, if $\tilde{x}_{2,g} = \tilde{x}_{1,g} + l^s_{1,g}$, $\tilde{s}_{1,g}$ is binding at its lower bound $l^s_{1,g}$, then by (3i) we have $\tilde{z}^{s,u}_{1,g} = 0$. Therefore, $-\tilde{\omega}_{1,g} = \tilde{z}^{s,l}_{1,g} \ge 0$ by (3b). Similarly, we have $\tilde{\omega}_{1,g} \ge 0$ when $\tilde{x}_{2,g} = \tilde{x}_{1,g} + u^s_{1,g}$. The update rules (5) and (6) will be used again later for the time period $(T+1)$ to perform sensitivity analysis.

Proposition 1 shows that the update rule (6) also enables the complementarity conditions to hold so the resulting point is a KKT point with respect to the horizon $\{2, \ldots, T\}$.

Proposition 1. *Let $(\tilde{x}, \tilde{s}, \tilde{\lambda}, \tilde{\mu}, \tilde{\omega}, \tilde{z}^x, \tilde{z}^s)$ be a KKT point of the initial horizon $\{1, \ldots, T\}$ problem. With the update rules of* (5) *and* (6)*, the point $(\tilde{x}, \tilde{s}, \tilde{\lambda}, \tilde{\mu}, \tilde{\omega}, \tilde{z}^x, \tilde{z}^s)$ restricted to the horizon $\{2, \ldots, T\}$ is a KKT point.*

We now introduce our two initialization methods for computing the starting values for the new variables at time period $(T+1)$.

Our first method initializes $(x_{T+1}, \lambda_{T+1}, \mu_{T+1}, z^x_{T+1})$ by duplicating the values from time period T. Other variables are initialized in a way that is consistent with those variables. We set the values of the ramping related variables to zero since the real power generator variable values are duplicated from the previous time period. In this case, ramping is not binding between time periods T and $(T+1)$.

This method is based on the intuition that if the change of the load is small between the two time periods T and $(T+1)$, then a solution to time period $(T+1)$ may be found near the previous one, a fact that we prove below.

Our second method sets the initial values of the new variables to a solution obtained from solving a much smaller subproblem: a single period optimal power flow (SPOPF) problem consisting of only the variables at time period $(T+1)$. This scheme is similar to the warm-start method of [11] in the context of model predictive control (MPC), although here we enhance the method by providing a sensitivity analysis stemming from the KKT residuals in Table I (with proofs in the Appendix [9]). When we formulate the subproblem, we place the ramp constraints in the form of the bound constraints on x_{T+1} as in (5), or we replace x_T with a constant $\tilde{x}_T$ in them. For the latter, the subproblem will be as follows:

$$\begin{aligned} \underset{x,s}{\text{minimize}} \quad & f(x), \\ \text{subject to} \quad & h(x) = d_{T+1}, \\ & c(x) \le 0, \\ & x_g - \tilde{x}_{T,g} = s_g, \ \forall g \in \mathcal{G}, \\ & l^x \le x \le u^x, l^s_g \le s_g \le u^s_g, \ \forall g \in \mathcal{G}. \end{aligned} \tag{7}$$

To accelerate its computation time for solving (7), we initialize its variable values to the values of the previous period variables, as the duplication method does.

The rationale for the SPOPF approach is (i) to compute a feasible primal initial point and (ii) to obtain an optimal

TABLE I
INITIAL KKT RESIDUALS OF OUR WARM-START METHODS.

Method	Initial error
Duplication	$\|\Delta d_T\| + \|\tilde{\omega}_{T-1}\|$
Single period OPF	$\|\hat{\omega}_T\|$

solution without solving the MPACOPF in the case where ramping is not binding in (7). In contrast to the duplication method, the SPOPF method finds a feasible primal point by solving (7). This may provide a better starting point when the load changes are not small. Regarding (ii), if the ramping is not binding, then it implies that the solution of (7) is independent of the previous time periods. Therefore, a solution to the MPACOPF is simply a concatenation of the previous solution and a solution to (7), that is, $x^* = (\tilde{x}_{2:T}, \hat{x})$ and $s^* = (\tilde{s}_{2:(T-1)}, \hat{s})$. For large examples, we may be able to save significant computation time in this case. The correctness of the solution will be verified in our error analysis later in this section.

Problem (7) might be infeasible, especially when the load change is large and the ramp limit is tight. In this case, we currently re-solve the problem without the ramp constraints. This still provides useful information: i) if it is infeasible again, then it implies that the MPACOPF problem is infeasible; (ii) otherwise, we have a feasible point for the new load so that we can warm-start and perform sensitivity analysis to evaluate the quality of our approximate scheme, as described in Section III.

B. KKT residual analysis of our starting points

The errors of our warm-start methods can be analyzed by computing their violations of Equations (3a) and (3c). Both initialization methods satisfy other equations by the way their values are constructed.

For the duplication method, the main source of error is the infeasibility of the power balance equation (3c) for the new load d_{T+1} and the multiplier for ramping $W_{T+1}(\omega_T)$ in (3a). Clearly, equations of (3) are satisfied up to time period T since we shifted the previous solution in time. Although $W_T(\omega)$ has changed from $E(\omega_{T-1})$ to $E(\omega_{T-1} - \omega_T)$, we set $\omega_T = 0$; hence (3a) is satisfied at time period T. For time period $(T+1)$, $h(x_{T+1}) = h(\tilde{x}_T) = d_T$. Thus the violation is $\Delta d_T := d_{T+1} - d_T$. In the case of (3a), we have $W_{T+1}(\omega) = E(\omega_T) = 0$. Since the equation was satisfied with $E(\tilde{\omega}_{T-1})$, the error is $\|\tilde{\omega}_{T-1}\|$. In summary, the total error is $\|\Delta d_T\| + \|\tilde{\omega}_{T-1}\|$. Note that if $\tilde{\omega}_{T-1} = 0$ (meaning that ramping is not binding between time periods $(T-1)$ and T), then the error is due solely to the load change.

For the SPOPF method, the error may arise from the term $\hat{\omega}_T$ from the solution of (7). With the same analysis as for the duplication method, the error is $\|\hat{\omega}_T\|$. This implies that if ramping is not binding between time periods T and $(T+1)$, that is, $\hat{\omega}_T = 0$, we can find a solution by just solving (7). Table I summarizes the errors of our initialization methods.

We make two observations based on our error analysis: (i) in addition to the load changes, only the ramp constraints contribute to the errors; and (ii) among the ramp constraints the ones in the tail (corresponding to time period $(T-1)$ and thereafter) determine the quality of our warm-start points. The first observation is intuitive and expected since only ramp constraints are intertemporal and link variables in different time periods. In case (ii), the error depends only on the load changes and the binding of the ramp constraint of (7). Thus, we may expect fast performance of our warm-start if the real power generator operation has enough margin with respect to the ramp limits in the tail.

III. APPROXIMATE METHODS

So far, we have assumed that a solution is to be computed to its optimality with respect to (3). In a real-time environment, however, where MPACOPF problems with a new load arrives every few seconds or minutes, this requirement may be too strong. Especially when the problem size is large, computing an exact solution may be much slower than the arrival interval of new problems so that operation may not be possible in a timely manner. While warm-start shows significantly faster performance than cold-start, as reported in Section IV, its computation time still may be too slow in this environment.

Instead of computing an exact solution for each time horizon, our approach is to try to approximately track the solution manifold by solving a truncated linear generalized equation (equivalently, a truncated quadratic program), which will be defined in Section III-A. Our warm-start point will be used as an initial point when we compute an approximate solution. Under some regularity assumptions, we show that the tracking error is bounded to the second order of the parameter changes. We emphasize that the parameter changes consist of only the changes in the last time period due to our warm-start. This is in comparison with the case where we do not shift the values in time. In that case, the parameter changes will involve the load changes of the whole time periods. Through experiments, we demonstrate that each approximate solution is computed fast enough to work in a real-time environment, while maintaining a good solution quality in a well-defined sense.

To analyze the quality of our approximation scheme, we use the theoretical results of strongly regular generalized equations (GEs) [7], [12]. Roughly speaking, the GEs represent a geometric version of the KKT conditions so that we can translate analytical results on the GEs into the ones on the KKT conditions. Strong regularity guarantees the desired behavior of GEs being stable to small perturbations. This property will be used to bound the distance between an exact solution and our approximate solution.

A. Strongly regular generalized equations

Under an appropriate constraint qualification, the first-order stationarity conditions of the following optimization problem with a given parameter p:

$$\begin{aligned} \underset{x}{\text{minimize}} \quad & f(p,x), \\ \text{subject to} \quad & h(p,x) = 0, \\ & g(p,x) \leq 0, \end{aligned} \tag{8}$$

can be written as

$$0 \in F(p, x, \lambda, \mu) + \mathcal{N}_K(x, \lambda, \mu), \tag{9}$$

where

$$F(p, x, \lambda, \mu) := \begin{bmatrix} \nabla_x f(p, x) + \nabla_x h(p, x)\lambda + \nabla_x g(p, x)\mu \\ -h(p, x) \\ -g(p, x) \end{bmatrix},$$
$$(x, \lambda, \mu) \in K := \mathbb{R}^n \times \mathbb{R}^q \times \mathbb{R}^v_+. \tag{10}$$

and

$$\mathcal{N}_K(y) := \begin{cases} \{z \mid \langle z, v - y\rangle \le 0, \forall v \in K\} & \text{if} \quad y \in K, \\ \emptyset & \text{if} \quad y \notin K. \end{cases} \tag{11}$$

(9) is called the generalized equation (GE) [12], and (11) is a normal cone to a closed convex set K at a point $y = (x, \lambda, \mu)$. One can easily verify that a KKT point of (8) is a solution to (9) and vice versa under a suitable constraint qualification.

For clarity of our analysis, we encapsulate all the primal/dual variables in y and parameters in p. In our case, parameter p represents the load and the lower/upper bounds of the real power generator variables at the first and last time periods. We note that the ordering of time periods is relative to the horizon; that is, if we are given the second time horizon problem, then the first period of it corresponds to time period 2 in the absolute sense.

Our problem is then equivalent to solving the following GE for a given parameter p:

$$0 \in F(p, y) + \mathcal{N}_K(y). \tag{12}$$

We are interested in the behavior of a solution of (12) near a point (p_0, y_0) subject to small perturbations of the parameter. To this end, we study the properties of its linear generalized equation (LGE) defined at (p_0, y_0) [7]:

$$T(y) := F(p_0, y_0) + \nabla_y F(p_0, y_0)^T (y - y_0) + \mathcal{N}_K(y). \tag{13}$$

Strong regularity [7] plays a critical role in enabling the solution to be well behaved. If it holds at a point (p_0, y_0), then we can bound the distance between its neighboring points. Let us define a residual by $r(p, y) := F(p_0, y_0) + \nabla_y F(p_0, y_0)^T (y - y_0) - F(p, y)$ and $y_i \in (T^{-1} \cap V)(r(p_i, y_i))$ for $i = 1, 2$, where V is some neighborhood of the origin. Then the distance between y_1 and y_2 is bounded by $L_\psi \|r(p_1, y_1) - r(p_2, y_2)\|$ with L_ψ being a local Lipschitzian constant of T. We note that $r(p_0, y_0) = 0$; therefore, the residual is small around (p_0, y_0). Combined with the KKT residual size analysis in Table I, the correspondent of r when moving from GEs back to KKT, this provides a mechanism for bounding the distance between an exact and an approximate solution.

In the case of an optimization problem (8), sufficient conditions are given in [7, Theorem 4.1] for the corresponding GE to be strongly regular: if LICQ and strong second-order sufficient conditions (SSOSCs) hold at a point (p_0, y_0), then it is strongly regular there. Since SSOCSs are assumed for virtually any algorithm for nonlinear programming, strong regularity of GEs requires no further assumptions compared with most other analyses. Note that when there are no degenerate indices, that is, there are no i's satisfying $g_i(x) = 0$ and $\mu_i = 0$ with μ_i being a multiplier for g_i, the SSOSCs become equivalent to the second-order sufficient conditions.

B. Approximately tracking a solution manifold consisting of strongly regular points

Strong regularity allows us to obtain a good approximation to a solution of nearby GEs by solving its associated LGE, a QP problem in our case. In [7, Theorem 2.3], it was shown that if (12) is strongly regular at (p_0, y_0) and $\nabla_y F$ is Lipschitz continous in both arguments, then for p near p_0 the distance between a solution $y(p)$ to (12) and a solution to the following LGE

$$r_\epsilon \in F(p, y_0) + \nabla_y F(p_0, y_0)^T (y - y_0) + \mathcal{N}_K(y), \tag{14}$$

with $r_\epsilon = 0$ is bounded to the second order of $\|p - p_0\|$. In [8, Theorem 4.1], the result was extended to hold for $r_\epsilon = O(\|p - p_0\|^2)$ so that a solution to a truncated LGE is enough to maintain a good solution quality.

Furthermore, in [8, Theorem 4.2] the authors showed that we can maintain stability of the tracking error: if y_p is a solution to (14) defined at $\bar{y}_0$ (called a reference point) close to a strongly regular point y_0 with $\|\bar{y}_0 - y_0\| \le \delta$ for some $\delta > 0$ in $O(\|p - p_0\|^2)$, then we will have $\|y_p - y(p)\| \le \delta$. Recursive application of this result, assuming that each exact solution $y(p)$ is strongly regular, implies that we can maintain stability of the errors to the second order of the parameter changes. The result also indicates that we can use y_p as our next reference (at which an LGE is formed) point to construct (14).

Based on these results, our approximation scheme first computes a warm-start point from the previous solution by shifting it in time and applying one of our warm-start methods, followed by the resolution of a truncated LGE (14), and continuing this procedure recursively in time. In the case of the first time horizon problem, where no previous solution is available, we solve it exactly.

To show the tracking stability of our approximation scheme, however, we do not directly apply the existing results since our reference point is constructed via shifting in time from the previous solution. Specifically, we do not have a guarantee that our reference warm-start point is also strongly regular and that it maintains the distance from the exact solution after shifting. We need to extend the results to take into account the shifting in time.

To this end, we first show that if y_0 is strongly regular with parameter p_0, then its shifted version $\tilde{y}_0$ with $\tilde{p}_0$ is also strongly regular. We then prove that if $\|y_p - y(p)\| \le \delta$ for some $\delta > 0$, then its shifted version also maintains the distance, that is, $\|\tilde{y}_p - \tilde{y}(p)\| \le \delta$. Based on these two results, the tracking error of the approximation scheme with our warm-start methods is shown to be bounded to the second order of the parameter changes. Note that these results hold independent of the time horizon length T.

Propositions 2–3 below present our theoretical results for the duplication method. For the SPOPF method, a separate

statement and its proof [9] are needed because its initialization procedure is different. In the propositions, we define a parameter for (2) to be $p = (l_1, u_1, l_T, u_T, d_{1:T})$, where (l_1, u_1) and (l_T, u_T) denote the lower/upper bounds of the real power generator variables at the first and the last time periods in a horizon in the relative sense, respectively, and d_i represents the load at the ith time period in the absolute sense.

Proposition 2. *Suppose that LICQ and SSOSCs hold at* $(\bar{x}, \bar{s}, \bar{\lambda}, \bar{\mu}, \bar{\omega}, \bar{z}^x, \bar{z}^s)$ *with parameter* $\bar{p} = (\bar{l}_1, \bar{u}_1, \bar{l}_T, \bar{u}_T, d_{1:T})$ *for* (2)*. Let* $(\tilde{x}, \tilde{s}, \tilde{\lambda}, \tilde{\mu}, \tilde{\omega}, \tilde{z}^x, \tilde{z}^s)$ *be the shifted warm-start point of the duplication method with its shifted parameter* $\tilde{p} = (\tilde{l}_1, \tilde{u}_1, \tilde{l}_T, \tilde{u}_T, d_{2:T}, d_T)$*, where* $(\tilde{l}_1, \tilde{u}_1)$ *and* $(\tilde{l}_T, \tilde{u}_T)$ *are obtained by applying the update rule* (5) *using* $\bar{x}_{1,g}$ *and* $\bar{x}_{T-1,g}$*, respectively, and* $\tilde{z}^x$ *is updated accordingly by using the update rule* (6)*. Then the warm-start point is a solution to* (2) *with parameter* $\tilde{p}$*. Furthermore, if (i) the vectors* $\begin{bmatrix}\nabla_x \tilde{h}(x) & \nabla_x c_{\mathcal{A}}(x)\end{bmatrix}$ *are linearly independent, where* $\tilde{h}(x)$ *is a duplicate of* $h(x)$ *excluding the real power generator variables and* $\mathcal{A}$ *denotes the set of indices of the active constraints of* c*; and (ii) for each* $t \in \{1, \ldots, T-1\}$ *and* $g \in \mathcal{G}$*,* $\tilde{x}_{t+1,g}$ *and* $\tilde{s}_{t,g}$ *are not active simultaneously, then it is a strongly regular point.*

Note that the shifted parameter $\tilde{p}$ in Proposition 2 may not correspond to the actual parameter values we need to use for the problem; the load at the last time period and $(\tilde{l}_T, \tilde{u}_T)$ may be different from the actual values, for example $d_T \neq d_{T+1}$ and $\tilde{l}_{T,g} \neq l^x_{T,g}$. These values are selected purely for sensitivity analysis purposes.

Proposition 3 shows that the shifting in time via duplication maintains the distance. In this proposition we use the infinity norm, $\|y - z\|_\infty := \max_i |y_i - z_i|$. Since the L_1, L_2 and the infinity norms are equivalent, the result holds for other norms.

Proposition 3. *Suppose that* $\|y - z\|_\infty \leq \delta$ *for some* $\delta > 0$*. Let* $\tilde{y}$ *and* $\tilde{z}$ *be their shifted versions obtained by applying the duplication method, respectively. Then* $\|\tilde{y} - \tilde{z}\|_\infty \leq \delta$*.*

We prove that the tracking error originated from computing an approximate solution is stable.

Proposition 4. *Assume that* (2) *is strongly regular at* y_0 *with parameter* p_0*. Let* $\bar{y}_0$ *be a reference point in the neighborhood* V *of* y_0 *(where the single-valued inverse function* $T^{-1} \cap V$ *is mapped) and* y_p *and* $y(p)$ *be solutions to the truncated LGE* (14) *defined at* $\bar{y}_0$ *with parameters* p_0 *and* p *and the GE with parameter* p*, respectively. Assume that the associated residuals satisfy* $\|r(p_0, \bar{y}_0) - r(p_0, y_0)\| \leq \delta_r$ *with* $\delta_r > 0$ *and* $\delta_r \in O(\|\Delta p\|^2)$*, where* $\Delta p = p - p_0$*, and there exists* $\delta_\epsilon > 0$ *satisfying* $\|r_\epsilon\| \leq \delta_\epsilon$*. If there exist* $\kappa > 0$ *and* Δp *satisfying*

$$\begin{aligned} \alpha_1 \|\Delta p\| \delta_r &\leq \kappa \|\Delta p\|^2, \\ (\alpha_2 + \kappa)\|\Delta p\|^2 + \delta_\epsilon &\leq \alpha_3 \delta_r, \end{aligned} \tag{15}$$

where α_1, α_2*, and* α_3 *are defined in the Appendix, then the tracking remains stable:*

$$\|\bar{y}_0 - y_0\| \leq L_\psi \delta_r \quad \Rightarrow \quad \|y_p - y(p)\| \leq L_\psi \delta_r.$$

TABLE II
STATISTICS OF DATA SET WITH $T = 10$.

Data	# Vars	# Constrs	Line (fr, to)	Generator
9	250	376	(4, 5)	2
30	710	1,454	(6, 10)	2
118	3,430	2,846	(24, 70)	89
RTS-GMLC	4,300	7,584	(101, 103)	101
300	7,370	6,621	(9005,9051)	76
1354pegase	32,270	58,060	(5019, 9112)	5490
2383wp	52,880	108,503	(346, 10)	18
9241pegase	213,710	323,705	(2169, 3124)	6857

Summing up, by Proposition 2 strong regularity is preserved under the duplication method. Proposition 3 guarantees that the distance will be within the same bound between the exact and approximate solutions via our duplication warm-start method. Proposition 4 shows that this recursive approximate LGE is stable: the tracking error (if initially small enough) is maintained and bounded by the second order of the parameter changes. By recursively applying the argument, we can keep track of the approximate manifold while the moving horizon with errors bounded by the second order of the parameter changes.

We note that the parameter changes involve two components: (i) the load changes between time periods T and $(T+1)$, and (ii) the distance from the actual bounds of the real power generator variable at time period T. The values of these two components can be controlled by the sampling rate (the time difference between adjacent time periods) and the ramp rate (the bound on variable s). The faster and the larger the sampling and ramp rates are, respectively, the smaller those two components are.

A similar argument holds for the SPOPF method as described in the Appendix [9]. In this case, we point out that the parameter changes have a single component, the distance from the actual bounds so it can be controlled by the ramp rate. Therefore, we may have tighter bounds between the exact and approximate solutions at the cost of solving the SPOPF problem.

IV. NUMERICAL RESULTS

In this section, we present computational results of our warm-start and approximate tracking methods described in Sections II and III, respectively. Table II[1] shows the statistics of the MATPOWER [13] and RTS-GMLC [14] (a modified version of RTS-96) data used to construct the MPACOPF model (2). We fix the length of the time horizon to $T = 10$, and each time period corresponds to a minute.

For our experiments, we assume an emergency situation where either a line or a generator has been off and, as a response, a moving horizon of the MPACOPF models is to be solved for emergency generator operation with $T = 10$ and $H = 20$, where H represents the number of times the time horizon moves forward one time period at a time. Therefore,

[1]The numbers of variables and constraints correspond to the case where a line has been off. They are similar in the generator-off case.

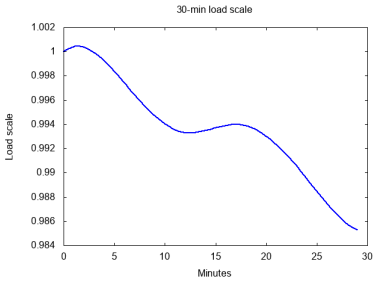

Fig. 1. 30-min load scale profile.

we provide a generator operation for the next 10 minutes for each time horizon, resulting in a total of 30-minute operation.

We chose a unit to turn off from a solution of an ACOPF problem, equivalently, an MPACOPF model with $T = 1$. To cut a non-redundant line, we chose a line having nonzero power flows at the solution. In the case of a generator, except for the 300-bus and RTS-GMLC cases[2], we chose the one with the largest real power. The last column of Table II shows the unit to turn off in each case. We note that the number in the generator column indicates the bus to which the offed generator was connected.

Our load data has been generated by multiplying a 30-min load scale to the load included in the original data. Hence, the proportion of the load among buses is the same as the given load proportion in the data file. Only the total load changes following the load scale. Figure 1 depicts our load scale profile. It has been generated from a five-minute system load profile for Oct. 2, 2018, obtained from the ISO New England website [15]. From the load profile, we picked 7:00 PM as our start time and computed the relative load scale for the next 30 minutes with one-minute granularity through interpolation. We note that the load dropped 1.5% from the start time over 30 minutes in this case.

We set the ramp rate to a value in a range from 0.04% to 1.0% per minute, except for RTS-GMLC data.[3] Our choice of ramp rate may be much smaller than the values currently being practiced in normal situations, but we chose it (a) to make sure that the ramp constraints are binding at our solution of the MPACOPF model and (b) in preparation of a future where the dispatchable ramp capacity is limited, as averaged over the entire system. If (a) does not occur, the SPOPF method will easily find an optimal solution, as discussed in the error analysis of Section II-B.

For the experiments of our approximate tracking scheme, we implemented a QP formulation of (14) and experimented with two versions of it: (i) solve it exactly ($r_\epsilon = 0$); and (ii) solve it approximately ($r_\epsilon > 0$) by setting the maximum number of iterations of the solver to a fixed number.

[2]The problem became infeasible when we chose the largest one in the 300-bus and RTS-GMLC cases. To avoid infeasibility, we chose the largest one among generators which output up to 100MW at the solution.

[3]The ramp rate was given in the RTS-GMLC data file, and the ramp constraints were binding at a solution with it. So we used the given ramp rate.

TABLE III
PERFORMANCE COMPARISON BETWEEN COLD- AND WARM-START WHEN A LINE HAS BEEN OFF.

Data	Average # Iterations and CPU Time in Sec		
	Cold-start	Duplication	SPOPF
9	52.68, 0.11	5.05, 0.01	2.00, 0.01
30	39.16, 0.37	8.63, 0.11	3.63, 0.06
118	28.05, 1.14	3.37, 0.13	1.74, 0.11
RTS-GMLC	44.79, 1.85	10.84, 0.66	8.11, 0.43
300	85.58, 8.82	5.58, 0.57	3.16, 0.43
1354pegase	61.95, 51.35	6.68, 5.82	4.74, 4.86
2383wp	70.58, 147.22	19.74, 46.31	17.05, 41.94
9241pegase	fail	143.58, 4378.57	125.11, 3852.90

TABLE IV
PERFORMANCE COMPARISON BETWEEN COLD- AND WARM-START WHEN A GENERATOR HAS BEEN OFF.

Data	Average # Iterations and CPU Time in Sec		
	Cold-start	Duplication	SPOPF
9	29.00, 0.07	7.47, 0.02	7.00, 0.02
30	55.26, 0.60	8.16, 0.09	4.47, 0.09
118	28.32, 1.04	3.21, 0.11	1.58, 0.07
RTS-GMLC	40.16, 2.14	6.95, 0.44	5.89, 0.35
300	64.32, 7.16	6.00, 0.52	2.79, 0.29
1354pegase	63.84, 48.84	7.58, 5.82	5.47, 5.02
2383wp	119.11, 364.46	31.16, 67.66	39.11, 89.23
9241pegase	fail	166.63, 4747.14	167.47, 4747.62

All experiments have been performed on a Linux machine having Intel Xeon CPU@2.30 GHz and 512 GB of memory. Julia 1.4.0, JuMP 0.18.6 [16], and Ipopt 3.2.10 [17] with MA57 [18] linear algebra engine and the number of threads of BLAS fixed to 1 were used to implement our methods. For warm-start, Ipopt's option has been set as follows. The option `warm_start_init_point` was set to `yes` to perform a warm-start, and options related to pushing the values into the interoir were relaxed so that we could start near the given point. This was achieved by setting all the parameter values pushing the given point into interior, such as `warm_start_bound_push` and `warm_start_bound_frac`, to 10^{-9}. We also set the `mu` strategy to `adaptive`. Our code and data are available at [9].

A. Performance of warm-start

Tables III and IV show the performance comparison between the cold- and warm-start methods. We present the average number of iterations and CPU time in seconds to solve each time horizon. We excluded the first time horizon problem from the average since all the three methods required an exact solution of it. Therefore, the average was computed over the 19 time horizons. For a fair comparison, we included the CPU time (but not the number of iterations) to solve the single-period problem (7) for the SPOPF warm-start method, although it was negligible compared with the overall CPU time. For the cold-start, we take a median of the lower and upper bounds of a variable as an initial point, because we use an interior point solver. For the phase angle variables, we initially set them to have the reference angle value.

As the results in Tables III and IV demonstrate, our warm-start method enabled us to achieve a significant performance

TABLE V
PERFORMANCE OF COLD-START WITH A POWER FLOW INITIAL POINT WHEN A LINE HAS BEEN OFF.

Data	Cold-start with a power flow initial point	
	Average # Iterations	CPU Time in Sec
9	21.63	0.06
30	25.74	0.25
118	23.68	1.21
RTS-GMLC	113.00	4.39
300	24.95	3.29
1354pegase	46.95	40.78
2383wp	62.00	136.33
9241pegase	178.53	9827.52

improvement and follow a more numerically stable solution path. Using warm-start, we computed a solution up to an order of magnitude faster than the cold-start. In the 9241pegase case, Ipopt showed severe numerical difficulties when we used the cold-start and was not able to solve the problem. Between the warm-start methods, the SPOPF method showed a better performance than the duplication method. We believe this is mainly because of primal infeasibility at the starting point of the duplication method caused by load changes.

Since the performance of the cold-start can be sensitive to a given initial point, we experimented with another initial point by setting it to a solution of the power flow equations. Table V presents the results when a line has been off. In most cases, we were able to obtain a better performance, but they still showed a much slower performance than our warm-start methods.

To see the performance variations between time horizons, Fig. 2 shows the distribution statistics of the iteration numbers over time horizons of the SPOPF method, when a line has been off. In the cases of RTS-GMLC, 2383wp, and 9241pegase, some variations were observed across iterations, however, most of them occurred near a solution performing a lot of iterations on looking for a numerically strict KKT point. This observation supports our expectation that our tracking scheme will provide a fast way of obtaining an approximate solution of good quality as described Section IV-B. Similar results were obtained for the duplication method.

B. Performance of approximate tracking scheme

Tables VI–VII present the performance of our approximate tracking scheme when we initialized the starting point using our warm-start methods with a generator turned off. In the tables, the fourth column is the average of the relative objective errors, and the fifth column represents the average constraint violation values.

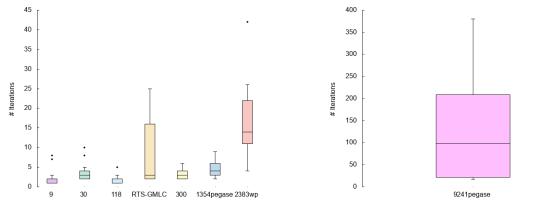

(a) 9 - 2383wp. (b) 9241pegase.

Fig. 2. Distribution statistics of the iteration numbers of the SPOPF method when a line was off.

TABLE VI
PERFORMANCE OF OUR TRACKING SCHEME WITH THE DUPLICATION WHEN A GENERATOR WAS OFF.

Data	# Max Iter	CPU (sec)	Rel Obj Err	Constr Viol
1354pegase	∞	2.72	5.55e-05	9.56e-03
	10	2.63	5.55e-05	9.56e-03
	5	1.67	6.10e-05	1.00e-02
	2	0.70	1.13e-04	1.34e-02
	1	0.42	6.56e-04	3.57e-02
2383wp	∞	38.42	1.13e-04	1.97e-03
	10	14.93	1.25e-04	1.99e-03
	5	8.03	2.33e-04	2.41e-03
	2	4.28	1.81e-03	8.42e-03
	1	2.33	2.44e-03	1.01e-02
9241pegase	∞	538.26	3.56e-05	1.53e-02
	10	316.88	3.56e-05	1.53e-02
	5	167.60	3.59e-05	1.53e-02
	2	99.19	3.05e-04	4.90e-02
	1	55.29	3.89e-04	7.30e-02

TABLE VII
PERFORMANCE OF OUR TRACKING SCHEME WITH THE SPOPF WHEN A GENERATOR WAS OFF.

Data	# Max Iter	CPU (sec)	Rel Obj Err	Constr Viol
1354pegase	∞	2.27	1.66e-09	6.28e-05
	10	2.36	1.66e-09	6.28e-05
	5	2.21	1.12e-09	6.28e-05
	2	1.20	1.43e-09	6.28e-05
	1	0.86	1.97e-09	6.29e-05
2383wp	∞	38.42	4.48e-07	1.35e-04
	10	17.26	6.83e-06	7.14e-04
	5	10.72	1.18e-05	3.05e-04
	2	6.94	1.95e-05	1.21e-04
	1	6.11	2.33e-05	1.25e-04
9241pegase	∞	439.69	3.46e-09	7.16e-05
	10	320.89	3.46e-09	7.16e-05
	5	174.16	3.45e-09	7.16e-05
	2	90.30	2.80e-09	7.16e-05
	1	62.48	3.03e-09	7.16e-05

Using our approximate tracking scheme, we were able to achieve a much faster computation time while maintaining a good solution quality. For the largest data set, 9241pegase, around two orders of magnitude speedup was achieved while keeping the relative objective errors negligible and the feasibility errors within 10^{-5} when we used the SPOPF warm-start. This allows us to provide a solution feedback of very good quality within 2 minutes for each time horizon. Similar results were obtained when we turned off a line.

Comparing Tables VI–VII, we note that both our approximate scheme and the SPOPF warm-start method have played a critical role in having a good approximate solution. We believe the feasibility guarantee and the consideration of the objective coefficients for the incoming time period makes the SPOPF method produce better results than the duplication method does.

C. Effect of load variations

We measure the effect of load variations on the performance of our warm-start under a whole load variation, i.e., all loads in a horizon are updated as the horizon moves forward. We would

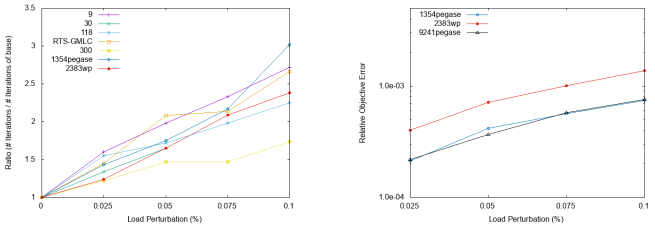

(a) Warm-start with duplication (b) Tracking with Max Iter 5

Fig. 3. Effect of load variations when a line has been off.

like to point out that our existing assumption – the forecasted loads in time periods between 2 and T do not change as the horizon moves forward in time to include a new period $(T+1)$ – is still a reasonable assumption for generator operation. In general, accurately reflecting the actual load is not possible, i.e., we do not know in advance exactly how much power will be used. Even though we update the forecast for the entire time periods as we move forward, we cannot guarantee that it will be more accurate than the previous forecast. It is generally admissible to have a discrepancy between the forecasted and actual loads, since the system inertia and primary frequency control [19] can tolerate a small imbalance between generation and load.

Fig. 3 shows the performance of the duplication warm-start method and its approximate tracking scheme for each load perturbation, when we turned off a line. We randomly perturbed the entire load in a horizon up to the value given in the figure, i.e., load$' = (1 \pm \text{perturb factor}) \times$ load, whenever a horizon moves forward. Since we assumed 1.5% change in load during 30 minutes, we chose 0.05% per minute as our median value for perturbations.

In both the warm-start and tracking scheme cases, performance deteriorated as we increased perturbations. However, the amount of degradation was not significant. In the case of the 1354pegase, the number of iterations has increased by 3 times for the largest perturbation (0.1%), but it was still much fewer than the base cases of the cold-start as described in Tables III and V.[4] The relative objective errors of our approximate scheme were not much different from the case where no perturbations were applied. Similar results were obtained for the constraint violations. We note that we did not present the 9241pegase case in Fig. 3(a) since we do not think one may want to employ a warm-start for it for a real-time optimization. Also, although we did not present, the SPOPF method was slightly worse than the duplication method. In this case, we think tailoring a solution for a single time period was not effective since the whole load in a horizon changed.

V. Conclusion

We have presented a real-time optimization strategy for solving a moving horizon of the MPACOPF problems. Our strategy consists of warm-start and an approximate tracking scheme. Warm-start provides a good initial point by exploiting the solution overlap between consecutive time horizons, and our tracking scheme allows us to approximately follow a solution path with errors bounded to the second order of the parameter changes of a single time period. This is achieved by solving a single QP for each time horizon either exactly or approximately. Experimental results over various networks of sizes up to a 9K bus system showed around two orders of magnitude faster computation time while maintaining very small feasibility errors.

[4]Similar results as in Tables III and V were obtained when we perturbed the load and used the cold-start.

References

[1] C. Y. Chung, W. Yan, and F. Liu, "Decomposed predictor-corrector interior point method for dynamic optimal power flow," *IEEE Transactions on Power Systems*, vol. 26, no. 3, pp. 1030–1039, 2011.

[2] J. F. Marley and I. A. Hiskens, "Multi-period AC-QP optimal power flow including storage," in *2016 Power Systems Computation Conference (PSCC)*, 2016, pp. 1–7.

[3] N. T. A. Nguyen, D. D. Le, C. Bovo, and A. Berizzi, "Optimal power flow with energy storage systems: single-period vs. multi-period model," in *2015 IEEE Eindhoven PowerTech*, 2015, pp. 1–6.

[4] V. Rao, K. Kim, M. Schanen, D. A. Maldonado, C. Petra, and M. Anitescu, "A multiperiod optimization-based metric of grid resilience," in *2019 IEEE Power Energy Society General Meeting (PESGM)*, 2019, pp. 1–5.

[5] K. Xie and Y. H. Song, "Dynamic optimal power flow by interior point methods," *IEE Proceedings - Generation, Transmission and Distribution*, vol. 148, no. 1, pp. 76–84, 2001.

[6] Y. Tang, K. Dvijotham, and S. Low, "Real-time optimal power flow," *IEEE Transactions on Smart Grid*, vol. 8, no. 6, pp. 2963–2973, 2017.

[7] S. M. Robinson, "Strongly regular generalized equations," *Mathematics of Operations Research*, vol. 5, no. 1, pp. 43–62, 1980.

[8] V. Zavala and M. Anitescu, "Real-time nonlinear optimization as a generalized equation," *SIAM Journal on Control and Optimization*, vol. 48, no. 8, pp. 5444–5467, 2010.

[9] Y. Kim and M. Anitescu. Appendix for a real-time optimization with warm-start of multiperiod AC optimal power flows. [Online]. Available: https://pages.cs.wisc.edu/~youngdae/rto

[10] J. Nocedal and S. J. Wright, *Numerical Optimization*, 2nd ed. Springer Science & Business Media, 2006.

[11] Y. Wang and S. Boyd, "Fast model predictive control using online optimization," *IEEE Transactions on Control Systems and Technology*, vol. 18, no. 2, pp. 267–278, 2010.

[12] S. M. Robinson, *Generalized equations and their solutions, Part I: Basic theory*. Berlin, Heidelberg: Springer Berlin Heidelberg, 1979, pp. 128–141.

[13] R. D. Zimmerman, C. E. Murillo-Sanchez, and R. J. Thomas, "MATPOWER: Steady-state operations, planning and analysis tools for power systems research and education," *IEEE Transactions on Power Systems*, vol. 26, no. 1, pp. 12–19, 2011.

[14] RTS-GMLC, "Reliability test system - grid modernization lab consortium." [Online]. Available: https://github.com/GridMod/RTS-GMLC

[15] ISO New England. Five-minute system demand. [Online]. Available: https://www.iso-ne.com/isoexpress/web/reports/load-and-demand/-/tree/dmnd-five-minute-sys

[16] I. Dunning, J. Huchette, and M. Lubin, "JuMP: a modeling language for mathematical optimization," *SIAM review*, vol. 59, no. 2, pp. 295–320, 2017.

[17] A. Wächter and L. Biegler, "On the implementation of an interior-point filter line-search algorithm for large-scale nonlinear programming," *Mathematical Programming*, vol. 106, pp. 25–57, 2006.

[18] HSL, "A collection of Fortran codes for large scale scientific computation." [Online]. Available: http://www.hsl.rl.ac.uk

[19] A. J. Wood, B. F. Woollenberg, and G. B. Sheblé, *Power generation, operation, and control*, 3rd ed. John Wiley & Sons, Inc., 2013.